Optics Letters

Noise-free terahertz-wave parametric generator

Sota Mine,* Kodo Kawase, and Kosuke Murate

Department of Electronics, Nagoya University, Furocho, Nagoya, 464-8603, Japan
**Corresponding author: mine.sota@b.mbox.nagoya-u.ac.jp*

Received 16 November 2021; revised 27 December 2021; accepted 24 January 2022; posted 24 January 2022; published 22 February 2022

We achieved noise-free terahertz (THz)-wave output from an injection-seeded THz-wave parametric generator (is-TPG) employing high-power injection seeding. A conventional is-TPG uses a weak continuous-wave (CW) seed beam. The position in which broadband noise is generated (via spontaneous parametric down-conversion) and the position of the THz signal overlap. Thus, the output features broadband TPG noise, reducing the signal-to-noise ratio. To solve this problem, we shifted the position in which the THz signal is generated to the front of the crystal; we separated the signal from broadband TPG noise using a high-powered, pulsed seed beam that was 10^7-fold more powerful than the CW seed beam. Thus, we extracted only the THz signal; we achieved a noise-free is-TPG. This system features a signal-to-noise ratio of 95 dB, approximately 40 dB better than the signal-to-noise ratio of the conventional system.

https://doi.org/10.1364/OL.448636

Terahertz (THz) waves find many applications in next-generation mobile communications [1], optical switching [2], electron acceleration [3], gas sensing [4], and nondestructive testing [5]. THz-wave sources have recently attracted considerable attention. The signal-to-noise ratio is of paramount importance. Both continuous-wave (CW) and quasi-continuous-wave (QCW) sources must be free from noise when providing single-frequency outputs, such as the resonant excitations of specific modes. The CW and QCW sources in the THz band include quantum cascade lasers and photomixers (photoconductive antennae). These sources improve the signal-to-noise ratio by removing phase noise [6] and optimizing the thickness of the photoconductive antenna semiconductor layer [7]. We previously developed an injection-seeded THz-wave parametric generator (is-TPG) as a QCW THz-wave source. An is-TPG is a unique tabletop THz source with high peak power (approximately 100 kW), wide tunability (0.4–5.0 THz), and a narrow linewidth that is Fourier transform-limited [8,9]. An is-TPG spectrometer has an ultra-wide dynamic range (up to 125 dB) during THz parametric detection [10]; this is the reverse of the is-TPG. We performed spectroscopic measurements through thick shields [11–13] and obtained three-dimensional images of plastics [14]. However, the THz-wave output contains weak broadband noise (broadband TPG noise) caused by spontaneous parametric down-conversion [15], although the power is approximately 10,000 times lower than that of the injection-seeded THz-wave (the THz signal). Complete suppression of broadband TPG noise creates an ideal QCW THz source with a high signal-to-noise ratio. We found that the THz signal and broadband TPG noise were generated at different positions, and used a new method to extract only the THz signal for noise-free THz output.

When a pump beam is injected into an $LiNbO_3$ crystal, pairs of weak broadband THz waves/Stokes beams are generated via Raman scattering through polaritons. Such a source is termed a TPG. Generation of THz waves requires a particular, nonlinear interaction length; the THz waves are amplified via three-wave nonlinear interaction between the Stokes and pump beams as they propagate along the x-axis of the crystal. THz waves are generated at the crystal position at which the oscillation threshold is exceeded. At this position, the parametric gain is concentrated using external seed beam injection to impart an initial excitation to the targeted Stokes wavelength. Thus, a single-frequency THz wave is created with an intensity >10,000-fold greater than the TPG. Tunability is wide; it is possible to ensure that the wavelength and angle of the seed beam satisfy the non-collinear phase-matching conditions. We term such a THz source an is-TPG. The conventional method used to reduce broadband TPG noise employs an iris to spatially extract only the THz signal under non-collinear phase-matching conditions [16]. This effectively removes broadband TPG noise, which affects detection, amplification, and generation [10,17]. However, the iris position varies according to the frequency of the THz signal. Furthermore, the iris does not completely block broadband TPG noise in the vicinity of the THz signal.

Here, we achieve a noise-free THz-wave output from an is-TPG by focusing on the positions at which the injection-seeded pure THz signal and broadband TPG noise are generated. Figure 1 shows schematics of both conventional and noise-free is-TPGs. In a conventional is-TPG, the THz signal and broadband TPG noise are generated at nearly identical positions because the seed beam is weak. In contrast, using a pulsed high-power seed beam [18,19], we found that the THz signal was generated at a position toward the front of the crystal [Fig. 1(b)]. Because broadband TPG noise was generated by only the pump beam, such noise was generated (as before) from the back of the crystal, regardless of whether the power of the seed beam was increased. Therefore, the THz signal (alone) could be removed from the $LiNbO_3$ crystal by adjusting the position of the Si-prism used for coupling between a crystal with a high refractive index and air. THz waves were extracted only where the coupler was crimped.

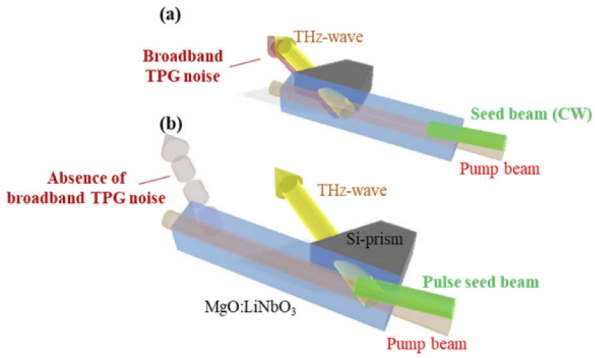

Fig. 1. (a) Conventional is-TPG featuring weak CW injection seeding. (b) Noise-free is-TPG featuring high-power injection seeding.

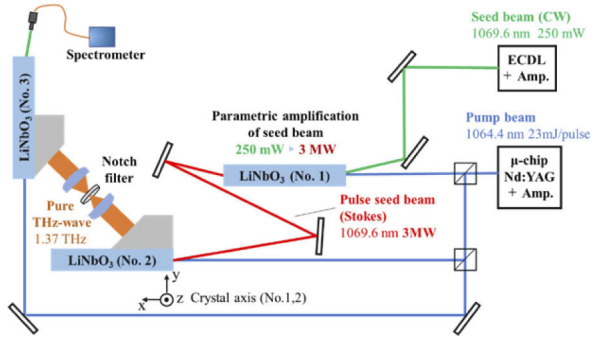

Fig. 2. Noise-free is-TPG using a pulsed seed beam.

Figure 2 shows the experimental setup for the noise-free is-TPG. We used $LiNbO_3$ crystals, 50 mm in length (numbered 1–3). The high-power seed beam was a Stokes beam generated using $LiNbO_3$ crystal 1. However, because it was difficult to separate the ordinary Stokes beam from the injection seed beam at the same angle, we used the Stokes beam generated on the opposite side of the pump beam (i.e., the Stokes beam generated by the reflection of the THz seed beam from the crystal *y*-surface) [20,21]. In principle, the energy and pulse widths of each Stokes beam are the same, and the monochromaticity (linewidth) is expected to be in the Fourier transform limit of ~4 GHz. A pulsed seed beam (a Stokes beam) of 300 μJ was obtained by injecting 3.5 mJ of a pump beam and 250 mW of a CW seed beam into $LiNbO_3$ 1. Because the Stokes beam width is approximately 25% of the beam pulse width, the Stokes beam pulse width was expected to be approximately 100 ps [8]; thus, the peak power was amplified 10^7-fold, compared with the CW seed beam power. The power stability of the pulse seed beam was around 1%. This set of pulse and pump beams was injected into $LiNbO_3$ 2 to generate THz waves. The Si-prism coupler was crimped to the front of the crystal [right-hand side of Fig. 1(b)] to ensure that only the THz signal was extracted (the length of the crimped surface of the Si-prism coupler on the $LiNbO_3$ crystal *y*-plane was about 3 cm.). The THz waves passed through lenses, then were injected into $LiNbO_3$ 3 (for detection). During detection, each THz wave was upconverted to a Stokes beam and observed using a near-infrared spectrometer ("THz parametric detection") [10]. The pump beam energies were 10 mJ for $LiNbO_3$ 2 and 3.0 mJ for $LiNbO_3$ 3.

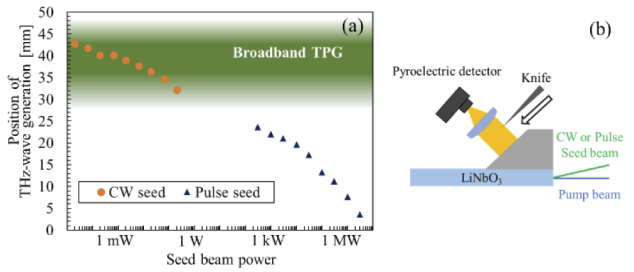

Fig. 3. (a) Positions of THz signal generation when using a CW or a pulsed-seed beam. The shaded area indicates the region of broadband TPG noise generation. (b) Measurement of THz-wave generation position using the knife-edge method.

Firstly, we used knife-edge measurements to compare the positions at which broadband TPG and THz signals were generated when inputting CW or pulsed seed beams [Fig. 3(a)]. For each measurement differing in seed beam intensity, the position of the Si-prism coupler was moved to where the THz wave was strongest. A knife was placed immediately after the Si-prism coupler; we used a pyroelectric detector to measure THz-wave intensity when the knife shifted. Based on the peak position, the generation position of the THz wave in the crystal was calculated from the generation angle. The circles show the positions at which conventional CW-seeded is-TPG signals were generated; the triangles show the positions of pulse-seeded is-TPG signals. The vertical axis shows the peak positions of THz-wave generation (i.e., the distances from the entrance to the $LiNbO_3$ crystal). The pulse seed beam power is the peak power. As shown in Fig. 3(a), the THz-wave generation position shifted to the front of the crystal (right-hand side of Fig. 1) as the seed beam power increased. This is because high-power seeding increases the growth rate of the THz wave and decreases the nonlinear interaction length required for amplification. The shaded area in Fig. 3(a) indicates the measured positions of broadband TPG noise generation. The THz signal from the CW-seeded is-TPG was generated from the rear of the $LiNbO_3$ crystal (left-hand side of Fig. 1), nearly identical to the position of broadband TPG generation. Conversely, the THz signal from the pulse-seeded is-TPG was generated at the front of the $LiNbO_3$ crystal (right-hand side of Fig. 1). Therefore, it was possible to spatially extract either the signal or the noise.

Next, to confirm the noise-free THz-wave output, we used a notch filter to suppress the THz signal alone; this revealed whether any weak TPG noise remained at the bottom. The notch filter was created by mixing 150 mg each of lactose (with a sharp absorption line at 1.37 THz) and polyethylene (Fig. 4), followed by pelleting. The filter was 13 mm in diameter and 1.8 mm in

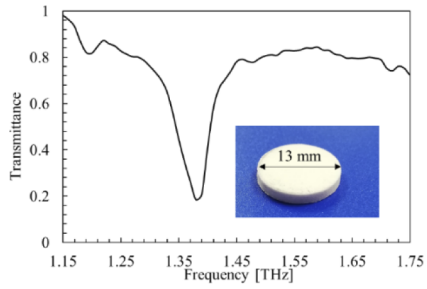

Fig. 4. Absorption spectrum of lactose. Inset shows a notch filter created using lactose and polyethylene.

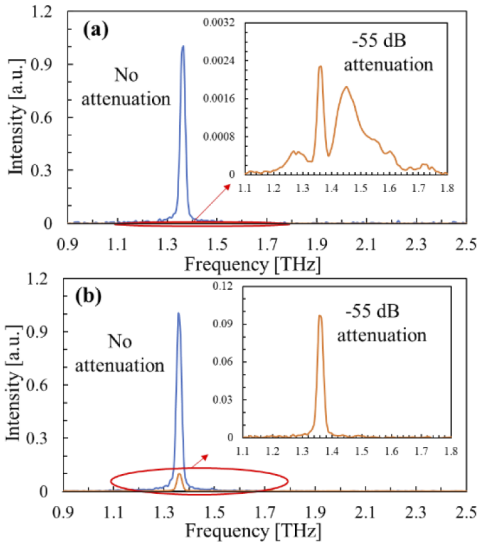

Fig. 5. THz spectra of (a) the conventional is-TPG and (b) the noise-free is-TPG. Insets show spectra derived after insertion of a notch filter featuring attenuation of −55 dB at 1.37 THz (a lactose filter). The *x*-axis shows the frequencies of the THz waves; the Stokes detection beam was a near-infrared beam.

thickness; it attenuated a 1.37-THz signal by –55 dB. We set the pure THz-wave frequency to 1.37 THz and inserted the notch filter at the focal point of Fig. 2 to attenuate only the THz signal. THz spectra are required when comparing a THz signal to broadband TPG noise; they are also required when calculating signal-to-noise ratios. We used the THz parameter detection method of Fig. 2; we derived the THz spectra by measuring the parameters of near-infrared detection Stokes beams upconverted from the THz waves.

Figure 5 shows the THz spectra of both the conventional and noise-free is-TPGs. The blue and orange lines are the THz spectra with and without the 1.37-THz −55 dB notch filter, respectively. The inset of Fig. 5(a) shows that broadband TPG noise was evident around the THz signal of the conventional is-TPG. Based on the parametric gain of $LiNbO_3$, there is usually a peak at around 2 THz. However, in this case, since the measurement frequency was optimized at around 1.37 THz, the center frequency of the noise also moved to a lower frequency. In contrast, as shown in the inset of Fig. 5(b), no noise was apparent in the pulse-seeded is-TPG. The THz-wave linewidths of the CW and pulse-seeded is-TPG were both approximately 4 GHz, as revealed by scanning Fabry–Pérot interferometry. Considering the limited resolution (approximately 20 GHz) of the spectrometer (S150-I-3648; Solar Laser Systems, Harrietsham, UK), the linewidths of the THz waves of Figs. 5(a) and 5(b) are broadened. No broadband TPG noise was observed, despite reduction of the THz signal to –95 dB (Fig. 6). Thus, the signal-to-noise ratio was 55 dB for the conventional is-TPG but more than 95 dB for the pulse-seeded is-TPG. The –90 dB and –95 dB filters were created by changing the lactose concentration of the notch filter shown in Fig. 4 to ratios of 95% and 100%, respectively. We also evaluated stability when THz spectrometry was combined with THz parametric detection (i.e., the stability of the Stokes detection beam). When we directly measured the THz-wave output from the is-TPG using a THz pyroelectric detector, there was no difference in stability between CW seeding and pulse seeding, which were around 1%; however, when the THz waves were attenuated more

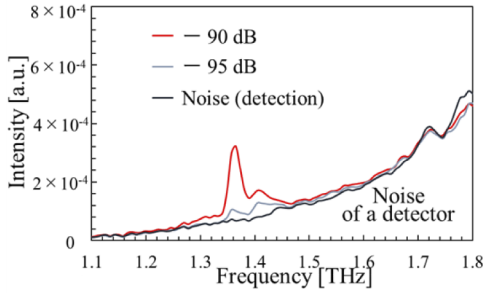

Fig. 6. THz spectrum of the noise-free is-TPG after insertion of a high-attenuation notch filter. No noise was observed, even at 95 dB of attenuation.

than –55 dB and detected by a THz parametric detector, a difference in stability was observed. The relative standard deviation stabilities were 7.0% for the conventional is-TPG and 1.7% for the pulse-seeded is-TPG. Parametric detection evaluates nonlinear optical effects; when impure THz waves are injected, stability deteriorates because of between-wavelength gain competition. However, we avoided this by suppressing noise; thus, the stability was much higher than when using the conventional is-TPG.

We achieved pure THz-wave generation using an is-TPG. In conventional is-TPG, broadband TPG noise and the THz signal are generated at the same position; thus, the THz-wave output contains a small amount of noise. We isolated the THz signal via high-power injection seeding; we extracted the THz signal by optimizing the position of the Si-prism coupler. The noise-free is-TPG performed better and was more stable than the conventional is-TPG. Our work will find applications in industry where high-precision quantitative measurements are required; it will also be useful in basic research concerning pure, high-intensity, widely tunable THz waves.

Funding. Japan Society for the Promotion of Science KAKENHI (18H03887, 19H02627); Foundation of Public Interest of Tatematsu; The Naito Science and Engineering Foundation.

Disclosures. The authors declare no conflicts of interest.

Data availability. Data underlying the results presented in this paper are not publicly available at this time but may be obtained from the corresponding author upon reasonable request.

REFERENCES

1. H. Sarieddeen, M.S. Alouini, and T.Y. Al-Naffouri, "An overview of signal processing techniques for terahertz communications," arXiv:2005.13176 (2020).
2. H. Hirori, A. Doi, F. Blanchard, and K. Tanaka, Appl. Phys. Lett. **98**, 091106 (2011).
3. E. A. Nanni, W. R. Huang, K. H. Hong, K. Ravi, A. Fallahi, G. Moriena, R. D. Miller, and F. X. Kärtner, Nat. Commun. **6**, 8486 (2015).
4. Y. Takida, K. Nawata, and H. Minamide, Opt. Express **29**, 2529 (2021).
5. H. Momiyama, Y. Sasaki, I. Yoshimine, S. Nagano, T. Yuasa, and C. Otani, Opt. Express **28**, 12279 (2020).
6. Y. Li, N. Yang, Y. Xie, W. Chu, W. Zhang, S. Duan, and J. Wang, Opt. Express **27**, 3146 (2019).
7. T. Göbel, D. Stanze, B. Globisch, R. J. Dietz, H. Roehle, and M. Schell, Opt. Lett. **38**, 4197 (2013).
8. S. Hayashi, K. Nawata, T. Taira, J. Shikata, K. Kawase, and H. Minamide, Sci. Rep. **4**, 5045 (2015).
9. K. Murate and K. Kawase, J. Appl. Phys. **124**, 160901 (2018).

10. H. Sakai, K. Kawase, and K. Murate, Opt. Lett. **45**, 3905 (2020).
11. M. Kato, S. R. Tripathi, K. Murate, K. Imayama, and K. Kawase, Opt. Express **24**, 6425 (2016).
12. R. Mitsuhashi, K. Murate, S. Niijima, T. Horiuchi, and K. Kawase, Opt. Express **28**, 3517 (2020).
13. K. Murate, H. Kanai, and K. Kawase, IEEE Trans. Terahertz Sci. Technol. **11**, 620 (2021).
14. S. R. Tripathi, Y. Sugiyama, K. Murate, K. Imayama, and K. Kawase, Opt. Express **24**, 6433 (2016).
15. G. K. Kitaeva, V. V. Kornienko, A. A. Leontyev, and A. V. Shepelev, Phys. Rev. A **98**, 063844 (2018).
16. M. Mohara, K. Shimura, K. Aiko, and T. Ono, in *Terahertz, RF, Millimeter, and Submillimeter-Wave Technology and Applications XIII* (SPIE, 2020), paper 112790X.
17. K. Murate, H. Sakai, and K. Kawase, IEEE Trans. Terahertz Sci. Technol. **10**, 200 (2020).
18. G. Tang, Z. Cong, Z. Qin, X. Zhang, W. Wang, D. Wu, N. Li, Q. Fu, Q. Lu, and S. Zhang, Opt. Express **23**, 4144 (2015).
19. W. Kong, Z. Li, Q. Yan, M. Zou, X. Zhou, and Y. Qin, J. Opt. Soc. Am. B **37**, 2479 (2020).
20. Y. C. Chiu, T. D. Wang, P. C. Wang, and Y. C. Huang, J. Opt. Soc. Am. B **36**, 42 (2019).
21. M. H. Wu, W. C. Tsai, Y. C. Chiu, and Y. C. Huang, Optica **6**, 723 (2019).